## ARTICLE IN PRESS

Mechanisms of Development xxx (2015) xxx-xxx

Contents lists available at ScienceDirect

### Mechanisms of Development

journal homepage: www.elsevier.com/locate/mod



# Volumetric tracking of migratory melanophores during zebrafish development by optoacoustic microscopy

Moritz Kneipp <sup>a,b</sup>, Héctor Estrada <sup>a</sup>, Antonella Lauri <sup>a,c,d</sup>, Jake Turner <sup>a</sup>, Vasilis Ntziachristos <sup>a,b</sup>, Gil G. Westmeyer <sup>a,c,d</sup>, Daniel Razansky <sup>a,b,\*</sup>

- <sup>a</sup> Institute for Biological and Medical Imaging (IBMI), Helmholtz Center Munich, Neuherberg, Germany
- <sup>b</sup> Department of Medicine, Technische Univeristät München, Munich, Germany
- <sup>c</sup> Institute of Developmental Genetics, Helmholtz Center Munich, Neuherberg, Germany
- <sup>d</sup> Department of Nuclear Medicine, Technische Universität München, Munich, Germany

#### ARTICLE INFO

Article history: Received 8 June 2015 Accepted 8 September 2015 Available online xxxx

Keywords: Melanocytes Tracking Optoacoustic microscopy Volumetric Label-free

#### ABSTRACT

Unveiling mechanisms driving specification, recruitment and regeneration of melanophores is key in understanding melanin-related disorders. This study reports on the applicability of a hybrid focus optoacoustic microscope (HFOAM) for volumetric tracking of migratory melanophores in developing zebrafish. The excellent contrast from highly-absorbing melanin provided by the method is shown to be ideal for label-free dynamic visualization of melanophores in their unperturbed environment. We established safe laser energy levels that enable high-contrast longitudinal tracking of the cells over an extended period of developmental time without causing cell toxicity or pigment bleaching. Owing to its hybrid optical and acoustic resolution, the new imaging technique can be seamlessly applied for noninvasive studies of both optically-transparent larval as well as adult stages of the zebrafish model organism, which is not possible using other optical microscopy methods.

© 2015 Published by Elsevier Ireland Ltd.

#### 1. Introduction

Comprehensive studies of the cellular and genetic mechanisms driving specification, recruitment and regeneration of melanophores have been instrumental to the understanding of a number of human disorders, including melanoma, vitiligo and hyperpigmentation (Yamaguchi and Hearing, 2014). The vertebrate zebrafish model organism (Danio rerio) has played a major role in these studies, as it offers a wide variety of genetic mutants exhibiting different pigmentation patterns with specific and well-characterized melanophore phenotypes (Rawls et al., 2001). In vertebrates, the melanophores develop from migrating neural crest cells (Nordlund, 2006) with their precursors spreading over the body early on during development. In zebrafish, the melanophores become visible between 24 and 27 h post fertilization (hpf), appearing at the edge of the developing neural tube (Taylor et al., 2011). Furthermore, optical transparency in its embryonic and larval stages makes the zebrafish model highly advantageous for early stage developmental studies (Rawls et al., 2001).

Imaging modalities that permit longitudinal monitoring of cellular events are key in performing developmental studies. Since melanophores exhibit strong optical contrast when compared to the rest of the transparent zebrafish embryo, optical methods have been

E-mail address: dr@tum.de (D. Razansky).

employed for both their visualization and manipulation. For instance, the behavior of normal and malignant human melanophores transplanted into zebrafish embryos was described (Lee et al., 2005). To study the regeneration and regulation of melanophores, zebrafish larvae have been irradiated using Q-switched lasers and imaged over an extended period of time (Yang et al., 2004). Additionally, timelapse microscopy studies have been used to investigate the differentiation of melanophores (Taylor et al., 2011).

Optical microscopy is however limited in its ability for label-free three-dimensional (3D) observations of cells while its penetration is further hindered by the intense light scattering in biological tissues, which limits noninvasive observations to the early stages of development and to applications using specific targeting dyes (Keller et al., 2008; Yang et al., 2004). Optoacoustic imaging has been shown to overcome the above limitations by employing high frequency ultrasound responses generated through short-pulsed light stimulation. Since ultrasound is not affected by the optical scattering in biological tissues, optoacoustics have been shown to achieve high resolution observations at depths of several millimeters to centimeters within tissues (Dean-Ben and Razansky, 2013b; Ma et al., 2012), thus enabling imaging of large highly diffuse specimen, such as adult zebrafish (Razansky et al., 2009), mice (Taruttis et al., 2010) and certain areas of the human body (Dean-Ben and Razansky, 2013a; Ma et al., 2012).

Here we assess the use of a hybrid focus optoacoustic microscopy (HFOAM) method (Estrada et al., 2014a; Estrada et al., 2014b) to volumetrically map the migration of melanophores *in vivo* during

http://dx.doi.org/10.1016/j.mod.2015.09.001 0925-4773/© 2015 Published by Elsevier Ireland Ltd.

<sup>\*</sup> Corresponding author at: Institute for Biological and Medical Imaging (IBMI), Helmholtz Center Munich, Neuherberg, Germany.

M. Kneipp et al. / Mechanisms of Development xxx (2015) xxx-xxx

their native development. The particular strengths of this approach is its intrinsic ability for fast three-dimensional observations as well as scalable resolution-at-depth, which allows for seamless translation of diffraction-limited optical resolution in shallow tissue layers into acoustic resolution performance in deeper optically diffuse tissues.

#### 2. Methods

#### 2.1. Experimental set up

The system used for the longitudinal imaging of melanophore development and *ex vivo* structural imaging is an adapted HFOAM scanner (Estrada et al., 2014b), shown in Fig. 1a. Signals are created by illuminating the target with 8 ns duration pulses (up to 10 KHz pulse repetition rate) at either 590 nm or 532 nm by means of a Dye Laser (Model: Credo; Sirah Lasertechnik GmbH, Grevenbroich, Germany) fed by a diode end pumped Nd:YAG Q-switched laser (Model: IS8II-E; EdgeWave GmbH, Würselen, Germany). The generated optoacoustic responses are acquired with acoustic resolution using a water-coupled spherically-focused PVdF transducer (Precision Acoustics, Dorchester, United Kingdom) with an active diameter of 6 mm, 7.8 mm focal length

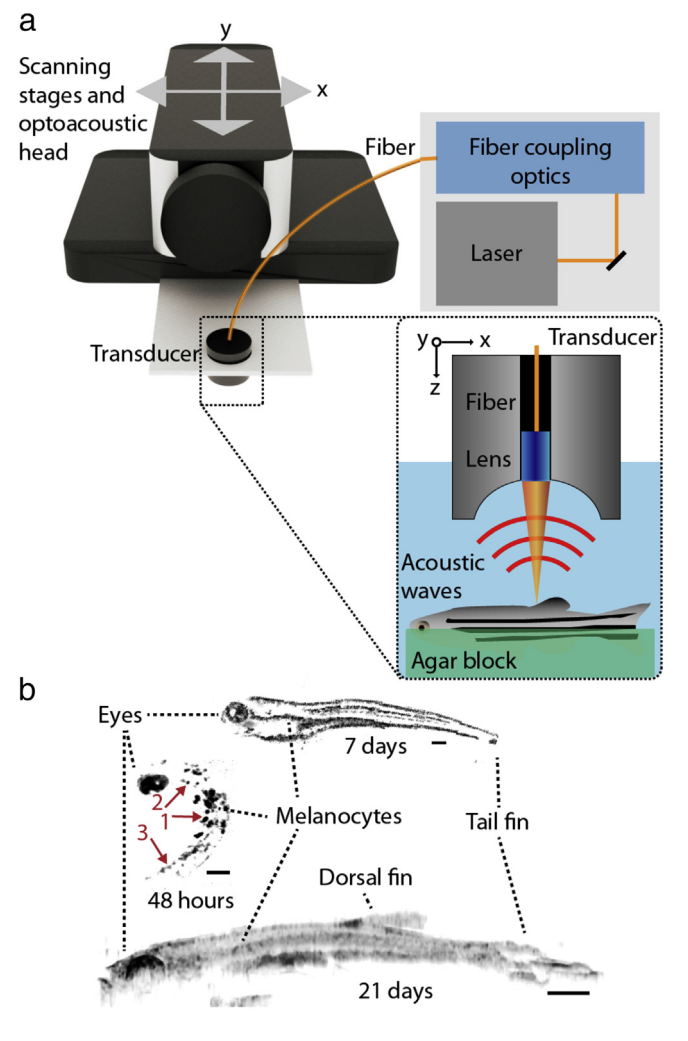


**Fig. 1.** Hybrid focus optoacoustic microscopy (HFOAM) setup and exemplary images obtained with the system. a: The scanning optoacoustic imaging head (zoom in) comprises a spherically-focused PVdF transducer and a GRIN lens assembly attached to a photonic crystal fiber. Samples are excited using a focused beam (labeled orange), with the resulting sound waves (labeled red) recorded by the transducer. Samples are typically fixed in agarose. b: The system can image fish through its developmental stages (lateral views of volumetric optoacoustic reconstructions are shown). Scale bars are 200 μm for the 48 hpf and 7 dpf and 1 mm for the 21 dpf reconstructions respectively. Red arrows mark the position of full width at half maximum (FWHM) measurements.

and ultrawideband frequency response centered around 30 MHz. Diffraction-limited spatial resolution around the acoustic focus of the transducer is 48 µm (Estrada et al., 2014a). Optical resolution is achieved by focusing the excitation beam through a Gradient-Index (GRIN) lens (Grintech GmbH, Jena, Germany) attached to the end of a single mode photonic crystal fiber. The fiber is inserted coaxially through an opening in the center of the transducer aperture, thus forming a diffraction-limited spot with a diameter of 21 µm at its full width at half maximum (FWHM) at a distance of 7.1 mm from the lens (Estrada et al., 2014b). By fast scanning of the optoacoustic imaging head in two lateral dimensions over the region of interest (ROI) and recording time-resolved signals, the acquired data is inherently three-dimensional. Depending on the field of view, the acquisition time for entire volumes with HFOAM is well below 1 min, whereas 2D imaging can be performed at a video rate (18 frames per second).

#### 2.2. Zebrafish maintenance and culturing

Zebrafish larvae were bred and maintained according to standard conditions (Westerfield, 2007). Fertilized eggs from AB wild type fish were raised in embryo medium at 28 °C. All procedures involving animals and their care conform to the institutional guidelines and with approval from the Government of Upper Bavaria.

#### 2.3. Imaging of developing and adult zebrafish

To ensure propagation of ultrasonic waves, the scanning head and the imaged samples were submerged in a small container filled with a suitable acoustic coupling medium. For the longitudinal tracking of melanophores during development, wild type (AB strain) zebrafish embyos around 26–27 h post fertilization were anesthetized in MS-222 (PharmaQ, Norway), dechorionated and embedded in 0.5% low melting agarose prepared with MS-222-treated fish water. The zebrafish embryos were imaged *in vivo* once per hour for a total duration of 8 h with a per pulse energy of 280 nJ.

In order to test the capability of the system to image an adult wild type fish (AB strain), the latter was euthanized, mounted in 1.2% low melting agarose and submersed into the imaging chamber filled with phosphate buffered saline solution (PBS). In this case, the total acquisition time for a volume of 200 mm<sup>3</sup> was in the range of 45 s.

#### 2.4. Pulsed laser phototoxicity tests

Since the efficient generation of optoacoustic responses implies utilization of nanosecond-duration laser irradiation, the in vivo phototoxicity tests were first conducted with 6 days old zebrafish larvae. For this, the latter were restrained in 1.2% agarose and imaged using different per pulse energies between 200 nJ to 10  $\mu$ J in order to evaluate the destructive nature of pulsed laser fluence on the melanophores. The light fluence on the surface of the fish was calculated by dividing the per pulse energy through the area of a disk with a radius of 10  $\mu$ m, corresponding to the FWHM size of the incident beam.

#### 3. Results

Before embarking on the *in vivo* developmental studies, we first tested the system's ability to image the different stages of zebrafish development, from embryonic to adult stages. As shown in Fig. 1b, at the early stage of 48 hpf, the eyes and individual melanophores are the first to generate detectable optoacoustic contrast. Scattered melanophores along the whole body length are visible at this stage. The red arrows in Fig. 1b mark the position of FWHM measurements of several melanophores in the youngest fish. The lateral FWHM was 25.98  $\mu$ m, 23.24  $\mu$ m and 29.22  $\mu$ m for the measurement points 1, 2 and 3 respectively. The volumetric nature of the imaging method allows for these measurements to be taken without the need to acquire

stacked images, regardless of the melanophore separation of around 380 µm in the z-dimension. At 7 days post fertilization (dpf), the melanophores have migrated to form the larvae's characteristic dorsal, lateral and ventral striped pigment patterns. Further, without the need to change any of the physical components of the system, imaging of adults at 21 dpf was possible with the same spatial resolution, see Fig. 1b. In the case of the adult fish, the wild type's pigmentation pattern can however adversely affect the achievable penetration depth through the reflective and absorbing characteristics of the silver and pigmented fish scales. Additionally, in the special case of adults, signals are no longer solely attributable to melanin. The increased amount of blood and other pigmentation gives rise to additional contrast not present in the images of the younger counterparts. The optoacoustic microscopy setup was however still able to acquire a 3D dataset of the adult fish in the same continuous manner as described above.

Fig. 2 showcases the particular benefit of using the 3D optoacoustic imaging approach versus traditional planar, two-dimensional microscopy. Using two-dimensional B-scan slices extracted from typical 3D optoacoustic scan data, signals originating from different depths in the tissue are clearly distinguishable. In contrast, the planar microscopy photographs merely represent the summed contribution of all signals in the depth direction. In particular, the planar microscopy image in Fig. 2a falsely shows a single stripe (labeled by a green arrow), whereas the volumetric optoacoustic data is able to reveal the true z-positions of several distinct melanophores, see Fig. 2b. This makes it possible to volumetrically track the individual melanophores, using our label-free 3D optoacoustic microscopy approach.

Despite the fact that the melanin pigment is highly absorbing in the visible range and therefore ideally suited for optoacoustic imaging, the high fluence attained by using a tightly focused illumination may cause irreversible pigment bleaching and cytotoxicity (Razansky et al., 2009). Thus, in order to reliably perform longitudinal studies in developing embryos, it was necessary to determine the optimal per pulse energies ensuring good optoacoustic signal levels while avoiding toxic effects on the cells. To this end, we illuminated 6 dpf zebrafish

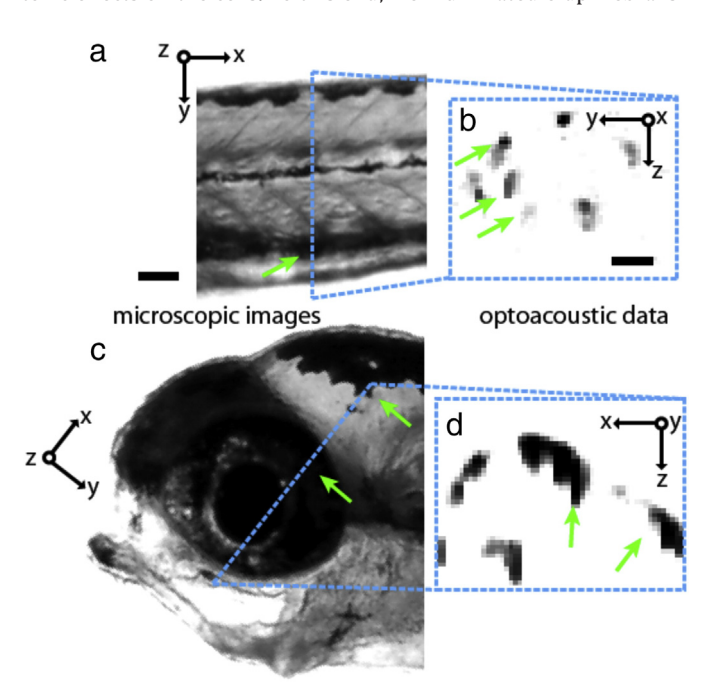
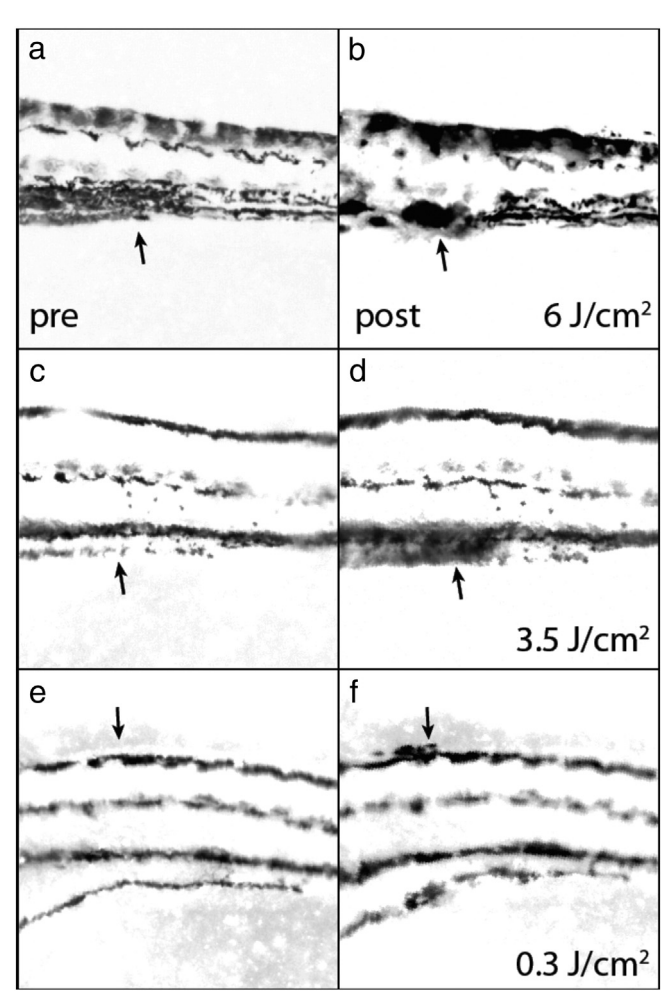


Fig. 2. Optoacoustic imaging yields true three-dimensional information a: In the blackand-white photograph of the zebrafish shown on the left, the green arrow marks an area where melanophores appear to form a stripe. The cross-sectional optoacoustic image through the labeled area (blue box) reveals the exact location (along the depth axis) of all the melanophores forming the stripe. b: Positions of melanophores in the eye in the depth direction are indistinguishable in the photograph. The optoacoustic slice reveals their relative position along the z-axis (blue box). Scale bar is 100 μm.

larvae with well developed pigmentation patterns at different per pulse energies and investigated the resulting damage, see Fig. 3. While later longitudinal *in vivo* experiments were run at safe fluence levels of 90 mJ/cm<sup>2</sup> (280 nJ per pulse), the system's illumination energy is scalable, achieving high enough levels to illicit phototoxic effects in melanophores. We found that fluence levels of 6 J/cm<sup>2</sup>, corresponding to the pulse energy of 19 µJ, are sufficient to cause visible damage to the melanophores in the zebrafish larvae. When comparing Fig. 3b to Fig. 3a, the signal from the melanin pigmentation appeared smeared, evincing significant cell damage. By reducing the fluence levels to 3.5 I/cm<sup>2</sup>, the effect of the pulsed laser radiation on the melanophores is significantly reduced with most pigmentation remaining intact and only minor destruction still observable, marked by arrows in Fig. 3c. Larvae appeared almost unaffected for fluence levels of  $0.3 \text{ J/cm}^2 - \text{per}$ pulse energy of ~1 uJ, where only minute changes could be recognized, marked by arrows in Fig. 3e,f.

Having determined the range of optimal per pulse energies for prolonged imaging sessions, we next investigated the possibility to longitudinally track migrating melanophore precursors with the hybrid optoacoustic microscope. Starting at approximately 27 hpf, once the first melanophores become visible under bright field microscopy, see Supplementary Fig. 1, we monitored the embryos for a total duration of 8 h, thereby including the time period during which migration and differentiation of melanophores has been reported (Taylor et al., 2011). In the time-lapse data shown in Fig. 4a, one can observe intense melanin signal in the center of the body — orange and green arrow in



**Fig. 3.** Pulsed laser induced-toxicity assay in zebrafish melanophores: a–f microscopic images of 6 days old zebrafish trunks before (a,c,e) and after (b, d, f) exposure to laser fluence of 6, 3.5 and 0.3 J/cm $^2$  for b, d, and f, respectively. Arrows mark areas with altered melanophores. Only minute changes are visible in f, upon close inspection.

M. Kneipp et al. / Mechanisms of Development xxx (2015) xxx-xxx

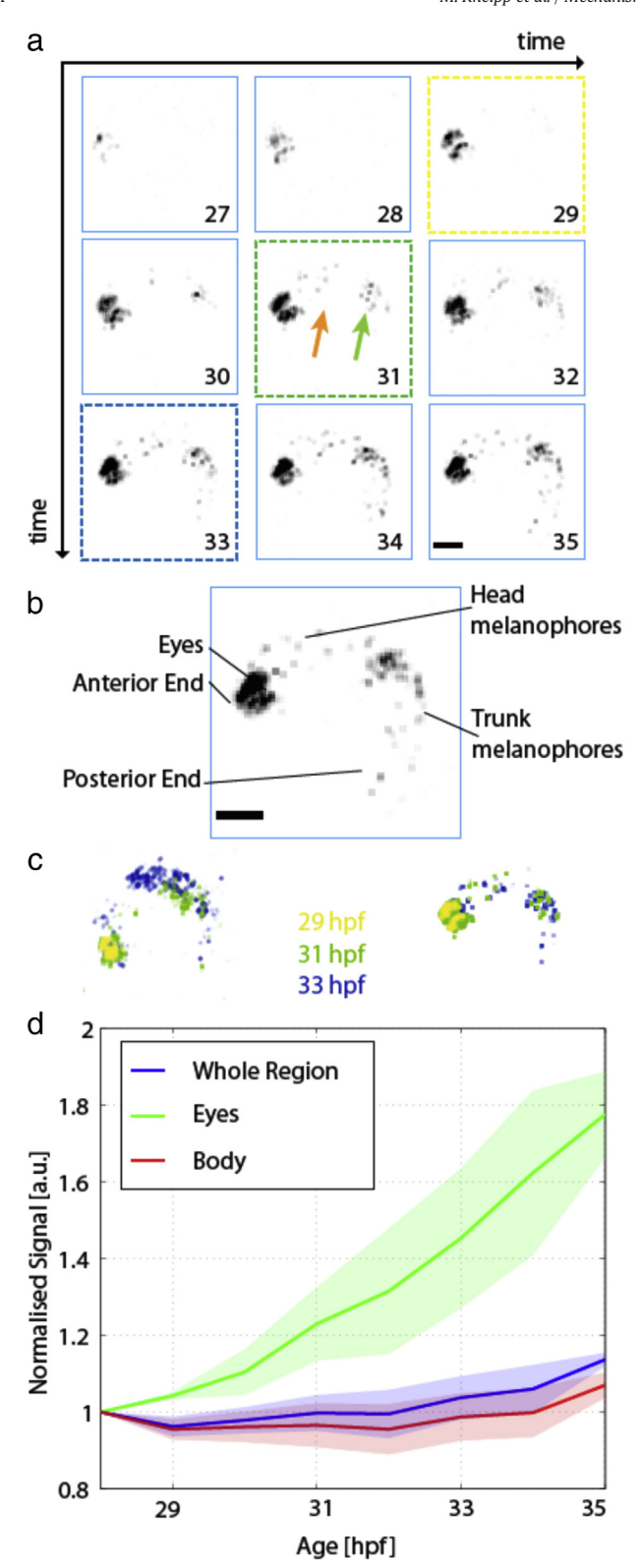


Fig. 4a, which likely corresponds to the mitf+ head and trunk neural crest-derived melanophore precursors. During further development, these precursors migrate and spread to cover the entire body of the embryo (Curran et al., 2009). The different anatomical regions identifiable from the optoacoustic images are labeled in Fig. 4b. Two examples of the typical observed melanophore development are further shown as color-coded time-lapse images in Fig. 4c, where colors correspond to different

time points. More specifically, it was possible to observe the expected increase of melanin content in the eyes at 29 hpf, yellow in Fig. 4c — corresponding frames in Fig. 4a exhibit the same color coding, followed by the gradual appearance and spreading of melanophores over the whole body, marked green and blue. At 31 hpf (green), the eyes have increased their pigmentation content. The overall melanophore position is concentrated around the focal spots of the head and trunk precursors. At 33 hpf (blue), the melanophores are continuing their migration over the whole body, and their spread is visible.

Finally, dynamics of the melanophore development are summarized in Fig. 4d where the normalized time-lapse optoacoustic signal curves are presented for different volumes of interest (VOIs) in 3 representative specimens. Here the signal increase originating from the eyes exhibits stronger increase when compared to the total VOI and the isolated body VOI. Note that as apposed to Fig. 4c, it is apparent from Fig. 4d that the signal increase in the eyes continues after 31 hpf. This can be explained by the fact that the physical extent of the eyes has remained constant between 31 and 33 hpf, the melanin content however continues to increase. The initial dip visible in the time trace may be due to the non-monotonic behavior of the melanophores spread and pigmentation, where melanophores appear and disappear during embryonic development (Rawls et al., 2001; Yang et al., 2004).

#### 4. Discussion

This study renders optoacoustic microscopy as an ideal tool for long-term label-free 3D imaging of developing zebrafish. Alternative approaches exist for 3D sectioning, namely confocal or multi-photon microscopy. However, these generally require fluorescence labeling of cellular structures to effectively distinguish the contrast of single melanophores, and/or drug-mediated aggregation of the melanin pigment to the center of the cell to avoid the light absorption that would prevent signal detection; moreover, they are not able to acquire significant volumes in real time. This has created the need for previous studies on melanophore development to resort to two-dimensional microscopy methods (Lee et al., 2005; McNeill et al., 2007; Mellgren and Johnson, 2004; Taylor et al., 2011; Yang and Johnson, 2006). As evident from the Supplementary Figure and Figs. 2a,c and 3 however, due to their susceptibility to photon scattering, planar microscopic images lack the scatter-free 3D contrast of optoacoustics in imaging melanophores and thus yield inferior results.

To fully exploit the potential of optoacoustic microscopy for *in vivo* studies of melanophore development, as well as other potential cells harboring specific optoacoustic constrast agents and follow their dynamics over time across entire organisms, safe illumination conditions should be implemented so that physiological events are not disturbed. Our phototoxicity experiments show that laser fluence levels below 300 mJ/cm² can be used for longitudinal tracking of zebrafish melanophores *in vivo* over an extended period of developmental time without arresting the development or causing major skin damage or significant bleaching. However, even the lower fluence levels of only 80 mJ/cm²,

**Fig. 4.** *In vivo* optoacoustic imaging of melanophores during development: a: time-lapse optoacoustic images (maximal intensity projections) of developing zebrafish embryo during melanogenesis and cell migration. The time interval between each snapshot is 1 h. The orange and green arrows mark the position of the head and trunk crest respectively. Scale bar is 200  $\mu m$ . b: Zoom in of the image at 35 hpf. Different anatomical regions and cells identifiable from the optoacoustic images are labeled. c: Color-coded time-lapse images for two different fish. The eyes are the first to express melanin (yellow). Signal then appears centralized around the putative region where head and trunk neural crest-derived melanophores originate, with the eyes reaching full pigmentation (green). The melanophores spread outwards to eventually cover the whole body (blue). Time points are also marked in (a) with color-coded dashed boxes. d: The mean optoacoustic signal of the fish increases over time for several areas. Standard error of the mean (n=3) is denoted for each curve by the shaded area.

M. Kneipp et al. / Mechanisms of Development xxx (2015) xxx-xxx

adopted in this study, were sufficient to generate high optoacoustic contrast over the entire duration of the longitudinal experiments.

Further, we were able to recapitulate the dynamics of melanophore expansion, originating from the respective precursors in the head and trunk regions, detecting the expected melanin-dependent signal increase over time. Altogether, these experiments set the ground for optoacoustics-based *in vivo* tracking of melanophores in zebrafish models. Future studies including larger cohorts could yield more specific insights into the dynamics of melanophores with regard to their pigment accumulation process, migration speed and possible preferred migration directions. This is made possible by the high temporal frame rate and high spatial resolution with whole volumes acquired in less than a minute at a spatial resolution of up to 21  $\mu m$ .

Further, our hybrid optoacoustic microscopy imaging method provides unparalleled scalability, both in terms of size of the imaged sample as well as the illuminating laser system, the latter being adjustable from non-destructive energies all the way to ablating energy levels (Yang et al., 2004). While the current system provides diffractionlimited optical resolution performance of 21 µm around the focal spot of the excitation beam, the spatial resolution can be readily adjusted to provide sub-cellular resolution performance by tighter focusing of the GRIN-lens-based beam delivery system. Clearly, tighter focusing and better spatial resolution will come at the cost of reduced field of view and/or scanning speed of the system. Additionally, the possibility to include multiple wavelengths in future studies may add spectral information to the data, thus delivering highly specific spectroscopic information of the underlying contrast. These abilities promise a wealth of possible applications in studying specific migration patterns, stimulusevoked responses, and melanohore regeneration in vivo. In particular, the ability to image and ablate in a single system (by varying pulse energy levels) allows for complex studies of lesion development and cell regeneration. Because of increasing interest in studying cell movements in tumor formation and dissemination, optoacoustic microscopy may become a valuable tool for label-free noninvasive observations of early and adult melanogenesis and migration of easily accessible animal model systems, such as zebrafish.

#### **Author contributions**

MK, AL, HE, GGW and DR developed the study. VN, GGW and DR supervised the study. MK, HE, AL and JT performed the experiments. MK, HE, and JT analyzed the data. MK, HE, AL, JT, VN, GGW and DR wrote the manuscript.

#### Acknowledgments

The study leading to these results has received funding from the European Research Council *ERC-2010-StG-260991* (D.R.). The authors further acknowledge grant support under *ERC-2012-StG\_20111109* (A.L. and G.G.W.), the Helmholtz Association of German Research Centers and the Technische Universität München.

#### References

- Curran, K., Raible, D.W., Lister, J.A., 2009. Foxd3 controls melanophore specification in the zebrafish neural crest by regulation of Mitf. Dev. Biol. 332, 408–417.
- Dean-Ben, X.L., Razansky, D., 2013a. Functional optoacoustic human angiography with handheld video rate three dimensional scanner. Photoacoustics 1, 68–73.
- Dean-Ben, X.L., Razansky, D., 2013b. Portable spherical array probe for volumetric real-time optoacoustic imaging at centimeter-scale depths. Opt. Express 21, 28062–28071.
- Estrada, H., Sobol, E., Baum, O., Razansky, D., 2014a. Hybrid optoacoustic and ultrasound biomicroscopy monitors' laser-induced tissue modifications and magnetite nanoparticle impregnation. Laser Phys. Lett. 11, 125601.
- Estrada, H., Turner, J., Kneipp, M., Razansky, D., 2014b. Real-time optoacoustic brain microscopy with hybrid optical and acoustic resolution. Laser Phys. Lett. 11.
- Keller, P.J., Schmidt, A.D., Wittbrodt, J., Stelzer, E.H., 2008. Reconstruction of zebrafish early embryonic development by scanned light sheet microscopy. Science 322, 1065–1069
- Lee, L.M., Seftor, E.A., Bonde, G., Cornell, R.A., Hendrix, M.J., 2005. The fate of human malignant melanoma cells transplanted into zebrafish embryos: assessment of migration and cell division in the absence of tumor formation. Dev. Dyn. 233, 1560–1570.
- Ma, R., Sontges, S., Shoham, S., Ntziachristos, V., Razansky, D., 2012. Fast scanning coaxial optoacoustic microscopy. Biomed. Opt. Express 3, 1724–1731.
- McNeill, M.S., Paulsen, J., Bonde, G., Burnight, E., Hsu, M.Y., Cornell, R.A., 2007. Cell death of melanophores in zebrafish trpm7 mutant embryos depends on melanin synthesis. J. Invest. Dermatol. 127, 2020–2030.
- Mellgren, E.M., Johnson, S.L., 2004. A requirement for kit in embryonic zebrafish melanocyte differentiation is revealed by melanoblast delay. Dev. Genes Evol. 214, 493–502.
- Nordlund, J.J., 2006. The Pigmentary System : Physiology and Pathophysiology. 2nd ed. Blackwell Pub, Malden, Mass.
- Rawls, J.F., Mellgren, E.M., Johnson, S.L., 2001. How the zebrafish gets its stripes. Dev. Biol. 240, 301–314.
- Razansky, D., Distel, M., Vinegoni, C., Ma, R., Perrimon, N., Köster, R.W., Ntziachristos, V., 2009. Multispectral opto-acoustic tomography of deep-seated fluorescent proteins in vivo. Nat. Photonics 3, 412–417.
- Taruttis, A., Herzog, E., Razansky, D., Ntziachristos, V., 2010. Real-time imaging of cardiovascular dynamics and circulating gold nanorods with multispectral optoacoustic tomography. Opt. Express 18, 19592–19602.
- Taylor, K.L., Lister, J.A., Zeng, Z., Ishizaki, H., Anderson, C., Kelsh, R.N., Jackson, I.J., Patton, E.E., 2011. Differentiated melanocyte cell division occurs in vivo and is promoted by mutations in Mitf. Development 138, 3579–3589.
- Westerfield, M., 2007. The Zebrafish Book. A Guide for the Laboratory Use of Zebrafish (Danio rerio). 5 ed. University of Oregon Press, Eugene.
- Yamaguchi, Y., Hearing, V.J., 2014. Melanocytes and their diseases. Csh. Perspect. Med. 4. Yang, C.T., Johnson, S.L., 2006. Small molecule-induced ablation and subsequent regeneration of larval zebrafish melanocytes. Development 133, 3563–3573.
- Yang, C.T., Sengelmann, R.D., Johnson, S.L., 2004. Larval melanocyte regeneration following laser ablation in zebrafish. J. Invest. Dermatol. 123, 924–929.